Eutectic reaction and oxidation behavior of Cr-coated Zircaloy-4 accident-tolerant fuel cladding under various heating rates

Dongju Kim [a,b,*], Martin Steinbrück [a], Mirco Grosse [a], Chongchong Tang [a], Youho Lee [b]

[a] Institute for Applied Materials IAM-AWP, Karlsruhe Institute of Technology, 76021 Karlsruhe, Germany
[b] Department of Nuclear Engineering, Seoul National University, 08826 Seoul, Republic of Korea

ARTICLE INFO

Keywords:
Eutectic
ATF
Cr coating
Heating rate
TGA
Oxidation heat

ABSTRACT

The Cr-coated zirconium alloy claddings are near-term approach for accident tolerant fuel (ATF) claddings. The performance of magnetron-sputtered Cr-coated zirconium alloys is investigated under conditions simulating severe accidents. The transient oxidation experiments were performed using a thermogravimetric analyzer (TGA) with five different heating rates (2–50 K/min) up to 1380 °C, which is above the Zr-Cr eutectic temperature. The weight gain of the Cr-coated specimens was found to be significantly lower than that of the uncoated reference up to approximately 1330 °C. However, after the occurrence of the Zr-Cr eutectic reaction and failure of the coating at 1330~1380 °C, the oxidation rate rapidly increased and the weight gain rate of the Cr-coated specimens was 1.5 to 10 times higher than that of the uncoated specimens. The difference was greater at higher heating rates. These results suggest that the Cr-coating has a limited effect in preventing oxidation and degradation of cladding in case of eutectic reaction. The oxidation was faster at higher heating rate, and it may even cause runaway oxidation of cladding due to the temperature rise caused by oxidation heat. These findings are important for understanding the capabilities and degradation behaviors of Cr-coated cladding under severe accidental scenarios.

1. Introduction

After the Fukushima accidents, there has been a strong need for accident-tolerant fuel (ATF) that can enhance resistance to high temperature oxidation and hydrogen generation during accidents like loss-of-coolant accident (LOCA). One of the most promising near-term options among the various ATF concepts is to use oxidation-resistant coatings on conventional zirconium-based alloy claddings. Chromium is the coating material currently actively investigated, which adheres well with a zirconium matrix, improve mechanical properties, have minimal impact on the neutron economy of the cladding tube [1,2], and provide high oxidation resistance by forming a protective layer of Cr_2O_3 on the surface [3–5].

Many studies have been carried out recently to investigate the high-temperature oxidation behavior of chromium coatings. They have found that the coating exhibits high oxidation resistance, but they have also noted the diffusion of chromium into zirconium and zirconium into chromium [6–9]. Chromium and zirconium diffuse in different ways. Chromium diffuses into the bulk zirconium matrix and zirconium does not diffuse into the bulk chromium, but it diffuses along the grain boundary of coating. The diffused zirconium could be oxidized if it reaches the Cr/Cr_2O_3 interface and it led to an oxygen influx into the unoxidized zirconium matrix, resulting in loss of protectiveness of coating. The diffusion of chromium can also cause several phenomena, such as the reduction in thickness of the chromium coating and the formation of a brittle $ZrCr_2$ layer. However, the most important phenomenon from a safety perspective is the Zr-Cr eutectic reaction between zirconium and chromium with the onset temperature of approximately 1330 °C [10], which is considerably lower than the melting point of zirconium (1855 °C).

Several investigations have been conducted to verify the high temperature behavior of coated cladding above the eutectic temperature. They reported that the Zr-Cr eutectic reaction occurs within the temperature range of 1300 to 1330 °C, and the protectiveness of coating is lost after the eutectic reaction.

Chaari et al. [11] conducted an experiment with Cr-coated M5 cladding under the heating rate of 20 K/min, and revealed that the eutectic reaction starts at 1308 °C for a 5 μm coating and 1328 °C for a 15 μm coating. Liu et al. [8]. and Steinbrück et al. [12] conducted oxidation tests on Cr-coated zirconium alloys and found that hydrogen

* Corresponding author.

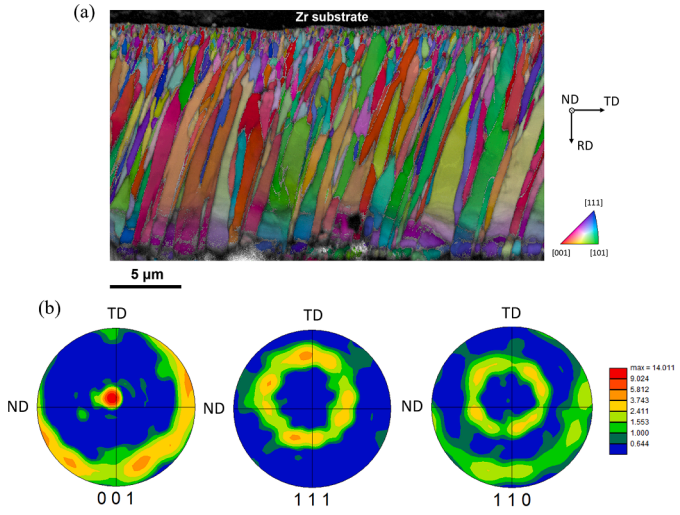

Fig. 1. EBSD analysis result for chromium coating of as-deposited specimen; (a) Inverse pole Fig. 2D map. (b) Pole figure.

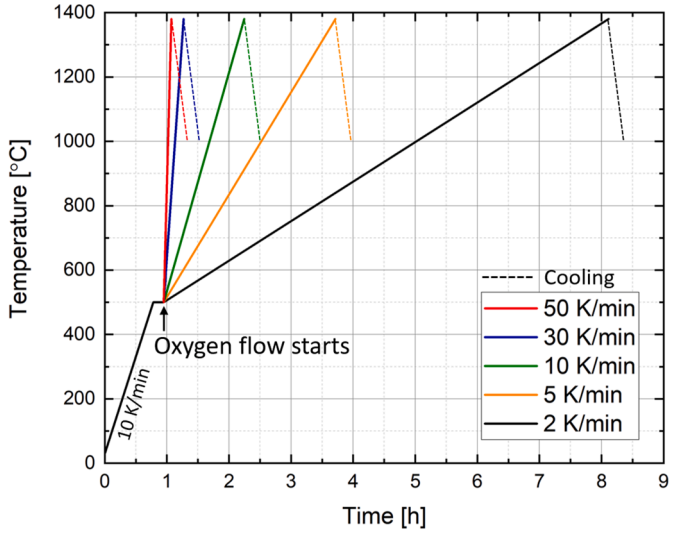

Fig. 2. Schematic temperature profile.

generation from the coated samples was significantly lower than that of the uncoated samples before the eutectic reaction. However, after the eutectic reaction, the hydrogen generation exceeded that of the uncoated samples. Brachet et al. [13] also found that the oxidation rate of Cr-coated samples increased after the eutectic reaction.

On the other hand, the eutectic behavior and subsequent oxidation under various conditions (e.g., heating rate) have not been systematically studied yet to the author's knowledge. Chromium and zirconium should exist in the form of a non-oxidized metal, and the chromium concentration should exceed the eutectic composition limit indicated by the phase diagram to cause a Zr-Cr eutectic reaction. Therefore, when a large portion of the coating is oxidized into the form of Cr_2O_3 or when chromium diffuses and exists as a solid solution with a concentration below the eutectic composition, the eutectic reaction may change. Extended exposure to oxidation, either with low heating rates during accidents or high degrees of pre-oxidation during steady-state operation, could lead to an increase in the portion of chromium that cannot take part in eutectic reactions.

In such a context, this study intends to examine how the heating rate affects the eutectic reaction of Cr-coated Zircaloy-4 claddings and subsequent oxidation. This study conducted additional experiments and

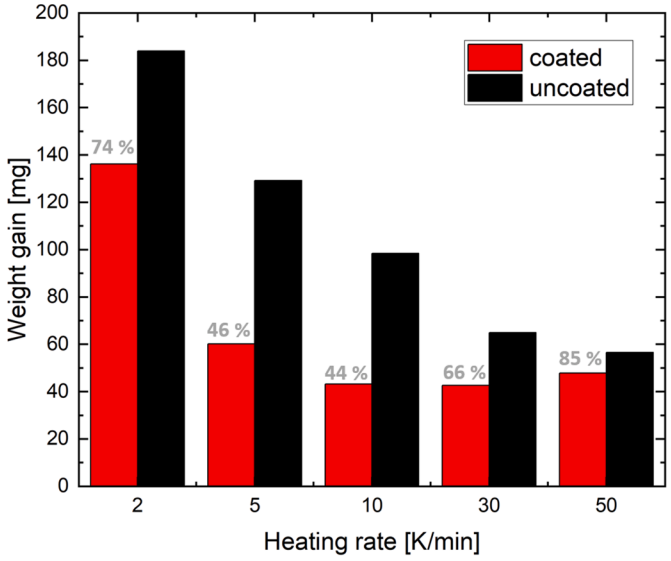

Fig. 3. Measured weight gain after transient oxidation of Cr-coated and uncoated Zircaloy-4 specimen.

discussion based on the result of previous study [14]. Transient oxidation experiments with five different heating rates (2–50 K/min) up to 1380 °C (above about 50 K higher than the Zr-Cr eutectic temperature) were conducted in an oxygen environment using a TGA. Weight gain of each specimen was in-situ measured, and after the experiment, further analysis was performed using several methods including scanning electron microscopy (SEM), energy-dispersive X-ray spectroscopy (EDS), and X-ray diffraction (XRD). The chromium protective layer is consumed by oxidation at the external surface and by chromium diffusion into the zirconium substrate. The influence of heating rate on chromium layer consumption is predicted using a model developed in past studies and compared with experimental results. The magnitude of heat generation due to rapid oxidation after the eutectic reaction was predicted.

2. Experimental method

2.1. Material

The transient oxidation experiments above the Zr-Cr eutectic temperature were performed using a Cr-coated Zircaloy-4 specimen, and for comparison, the uncoated Zircaloy-4 specimens. The uncoated specimen is in plate shape (15 mm × 10 mm × 0.65 mm) and the base material is Zircaloy-4 (Zr-1.5Sn-0).2Fe-0.1 Cr). A 17 μm thick pure chromium coating was applied to both sides of the Zircaloy-4 specimen using magnetron sputtering [15]. The microstructure of as-deposited chromium coating has been characterized by Electron Back Scatter Diffraction (EBSD) analysis using JEOL JSM-7600F with Oxford instruments Symmetry CMOS type EBSD detector. Fig. 1(a) is EBSD 2D map with grain structure and orientation (inverse pole figure). The coating exhibits a columnar structure, and the grain width was about a few hundred nanometers (<300 nm) at the interface with Zr substrate and about a few microns (<2 μm) near the coating surface. The coating was dense without void or cracks. Fig. 1(b) is pole figure for the chromium, and it shows that the predominant crystal direction of coating is about 15° tilted [001] texture from perpendicular to the sample surface.

2.2. Experimental procedure

TGA equipment (NETZSCH STA449 F3 Jupiter) was used to carry out the transient oxidation experiments; the schematic temperature program of each experiment is given in Fig. 2. Each specimen was heated to

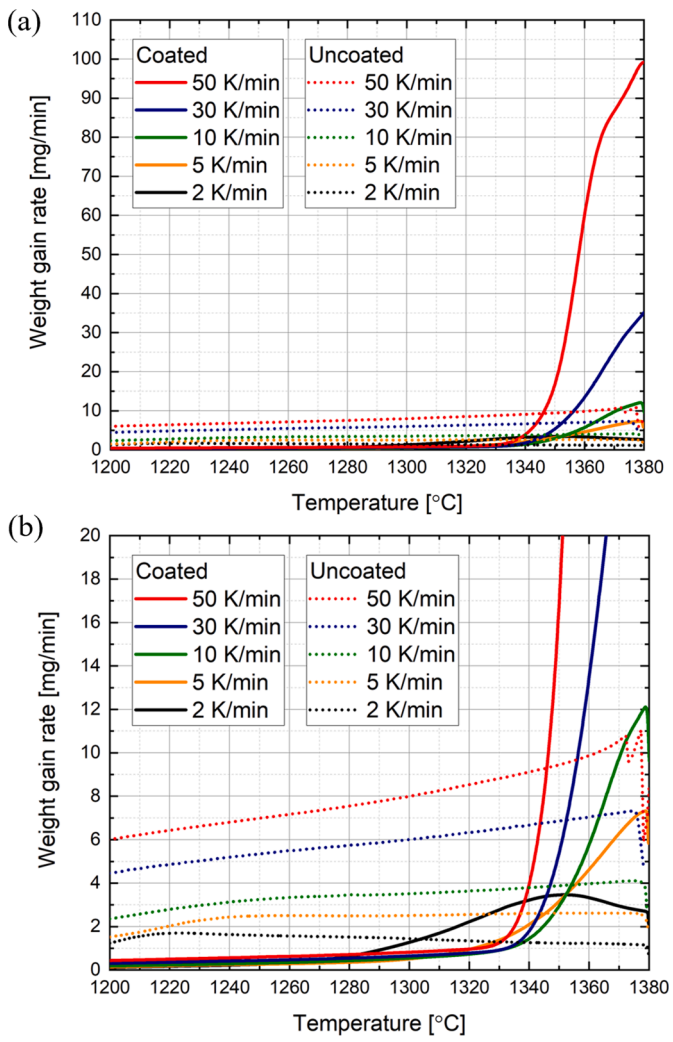

Fig. 4. The weight gain rate during the oxidation of both Cr-coated and uncoated Zircaloy-4 specimens for various heating rates; (a) The full range. (b) Magnified for the 0–20 mg/min range.

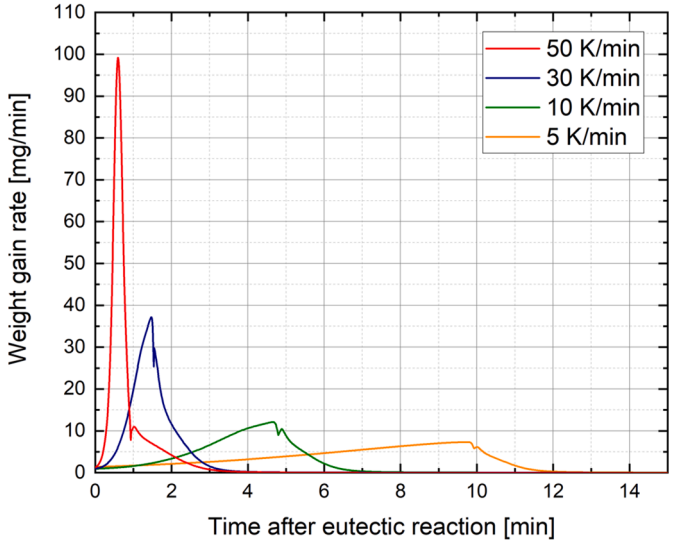

Fig. 5. The post-transition(eutectic reaction) weight gain rate of Cr-coated specimen.

up to 500 °C under argon gas environment with a heating rate of 10 K/min and kept isothermally for 10 min to stabilize. Thereafter, the specimen was heated up to target temperature (1380 °C, about 50 K above eutectic temperature) under argon/oxygen mixture ($\dot{V}_{Ar}$ 20 *ml/min* & $\dot{V}_{O_2}$ 50 *ml/min*) with five different heating rates (2, 5, 10, 30, and 50 K/min). Each specimen was naturally cooled down under argon gas environment after reaching the target temperature, and the cooling rate during the initial cooling stage (1380~1000 °C) was measured to be approximately 80 K/min.

The mass change of each specimen during the experiment was in-situ measured by the balance in TGA equipment (accuracy: 0.1 μg). After the test, the post-test appearance of specimen was examined, and the surface morphology and phases formed on the surface were characterized using SEM and XRD. The post-test microstructure of the specimens was examined using SEM and EDS.

3. Results

3.1. Weight gain

The weight gain during the oxidation of Cr-coated and uncoated specimens was compared for each heating rate and is depicted in Fig. 3. It is noteworthy that the uncoated specimen shows a higher weight gain than the coated specimen under the same condition due to the oxidation resistance of the chromium coating. The oxidation time is shortened at higher heating rates, hence, the weight gain of the uncoated specimen tends to decrease as the heating rate increases. On the other hand, coated specimens showed the same trend in the range of 2–10 K/min heating rate, but the weight gain of the 50 K/min specimen was larger than that of the 10 or 30 K/min specimen despite a shorter oxidation time. The difference between the uncoated specimen and the coated specimen was smallest for 50 K/min specimens of about 15%.

The weight gain rates during the oxidation of Cr-coated and uncoated specimens for each heating rate are depicted in Fig. 4. It is noteworthy that for the coated specimen, escalation in the weight gain rate was observed at a certain temperature while there was no significant change according to the temperature for the uncoated specimen as can be seen in Fig. 4(a). As can be seen in the magnified weight gain rate (Fig. 4(b)), escalations in the weight gain rate of the Cr-coated specimen with a heating rate of 5–50 K/min were in the range of 1330–1340 °C, which indicates the failure of coating due to the Zr-Cr eutectic reaction. On the other hand, the Cr-coated specimen with a heating rate of 2 K/min, which is the lowest heating rate, shows a transition in weight gain at around 1280 °C and no additional escalation after the Zr-Cr eutectic temperature (~1330 °C). The transition at around 1280 °C seems to be due to the diffusion and oxidation of zirconium to the Cr/Cr_2O_3 interface accompanying oxygen influx to the zirconium matrix [16].

The post-transition weight gain rate following the Zr-Cr eutectic reaction of the Cr-coated specimen at different heating rates (5–50 K/min) is depicted in Fig. 5. The transition time was determined using the analysis of NETZSCH software. The slope and maximum value of the weight gain rate tend to increase with the heating rate.

3.2. Surface characterization

Fig. 6 shows the appearance of each sample after the test. In the case of uncoated specimens (Fig. 6(f)-(j)), there was no significant change in surface morphology with the heating rate. There was a slight difference in surface color depending on the degree of oxidation. On the other hand, in the case of coated specimens, there was a remarkable change in surface morphology with the heating rate. The local swelling due to volume change during solid to liquid transition and surface tension of the melt made an uneven surface, the so-called "crocodile skin" shape, which can be easily found in the specimen with eutectic reaction [12, 13]. As can be noted in Fig. 6, the characteristic "crocodile skin" shape

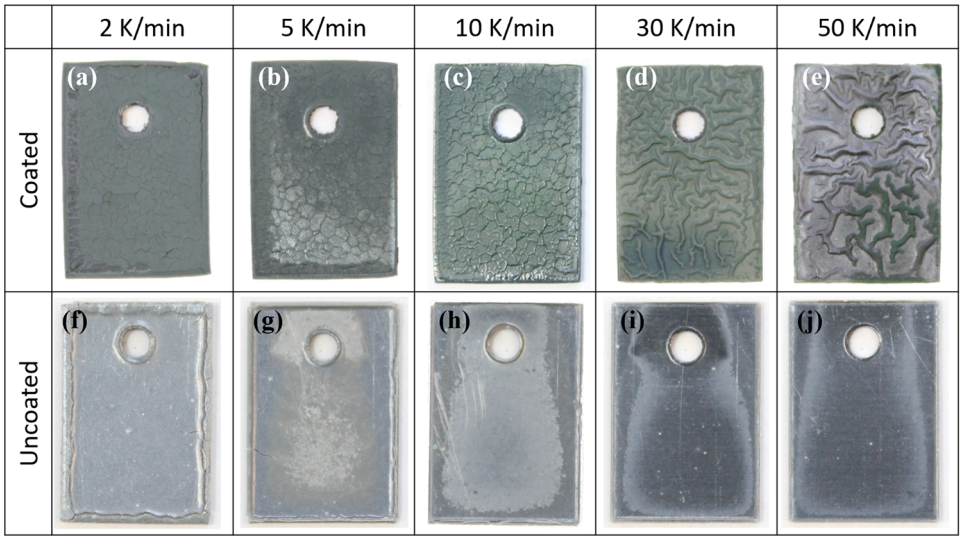

Fig. 6. Post-test appearance of specimens.

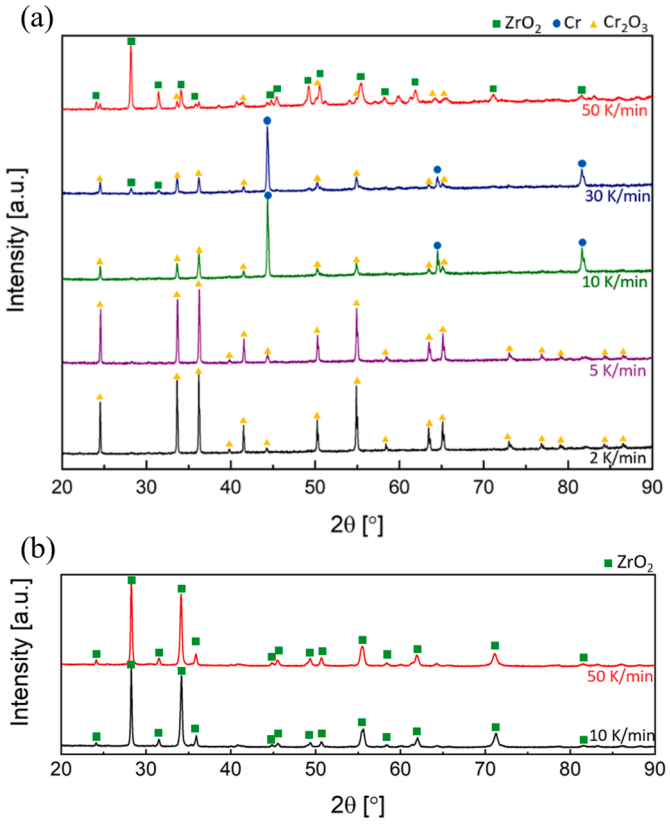

Fig. 7. The XRD spectra and identified phases; (a) Cr-coated Zircaloy-4 specimen. (b) Uncoated Zircaloy-4 specimen.

can be identified for Cr-coated specimens and was more pronounced for the higher heating rate.

Fig. 7(a) and (b) show the surface XRD spectra of Cr-coated specimens and uncoated specimens, respectively. In the case of Cr-coated specimens, all diffractograms include an XRD peak of the Cr_2O_3 phase in common, but the existence of XRD peaks of other phases (e.g., ZrO_2, Cr) was different according to the heating rate. The diffractograms of specimens with a heating rate of 2–5 K/min only include the Cr_2O_3 peaks. In the case of specimens with a heating rate of 10 and 30 K/min, their diffractograms also include pure chromium peaks and in the case of specimen with heating rate of 30 and 50 K/min, their diffractograms also include ZrO_2 peaks. In short, the surface of specimens with low heating rate mainly consists of a Cr_2O_3 layer while that of high heating rate include chromium and/or ZrO_2 phases.

3.3. *Microstructure characterization*

Fig. 8 shows cross-sectional backscattered electron (BE) SEM images and EDS mapping results of each element (chromium, zirconium, and oxygen) of Cr-coated specimens for different heating rates and uncoated specimen with heating rate of 10 K/min. As can be noted, a Cr_2O_3 layer was formed on both outermost sides of all tested conditions, which is consistent with the results from XRD measurement. However, in the case of specimens with a high heating rate, especially 50 K/min, the thickness of the chromium oxide layer is relatively thin and cannot be found in some areas. The ZrO_2 layer was formed between the Cr_2O_3 layer and a metallic layer consisting of zirconium and chromium, which indicates the failure of coating and loss of protectiveness. The specimen with 2 K/min, which has the largest weight gain, showed the thickest ZrO_2 layer of about 184 μm. The uncoated specimen (Fig. 8(f)) has the microstructure of a typical oxidized zirconium specimen, with ZrO_2 layer formed on both outer surfaces.

It is noteworthy that all coated specimens showed a chromium-rich region in the zirconium matrix as indicated in EDS mapping results, but the microstructures differ by heating rate. Further analyses of the chromium-rich region were conducted and are presented in Appendix A. It shows that the specimen with weight gain escalation near the Zr-Cr eutectic temperature (Fig. 8(b)-(e)) has a typical post-eutectic structure that zirconium and $ZrCr_2$ intermetallic phase were mixed (Zr-$Cr_{prior\ eutectic}$), and fine chromium precipitation that did not participate in the eutectic reaction coexists at the center (Fig. A1). In addition to that, local volume change occurred due to liquid to solid transition during cooling. The extent of Zr-$Cr_{prior\ eutectic}$ and the degree of local swelling tend to be greater for specimens with high heating rates.

On the other hand, there was no Zr-$Cr_{prior\ eutectic}$ structure in the Cr-coated specimen with a heating rate of 2 K/min (Fig. 8(a)), instead, it has relatively large chromium precipitates at the center. The averaged chromium content in non-oxidized zirconium is about 1.7 wt%, which is smaller than the composition limit (Fig. 11). It is assumed that no eutectic reaction has occurred, which is consistent with the weight gain result that no escalation around eutectic temperature was observed (Fig. 4(b)).

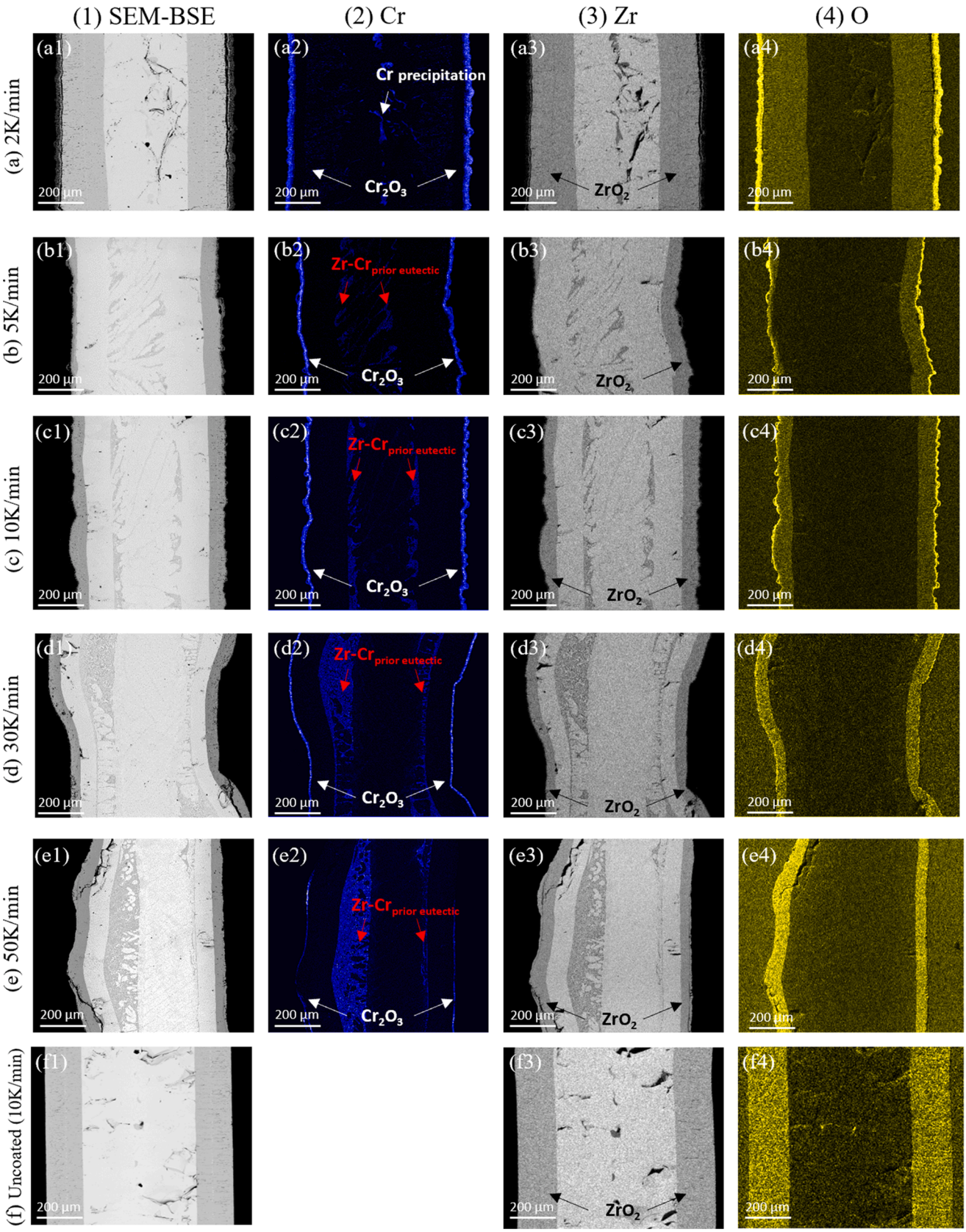

Fig. 8. The cross-sectional SEM-BSE images and EDS mapping results (chromium, zirconium, oxygen); Cr-coated (2–50 K/min) specimens ((a)-(e)). Uncoated (10 K/min) specimen (f).

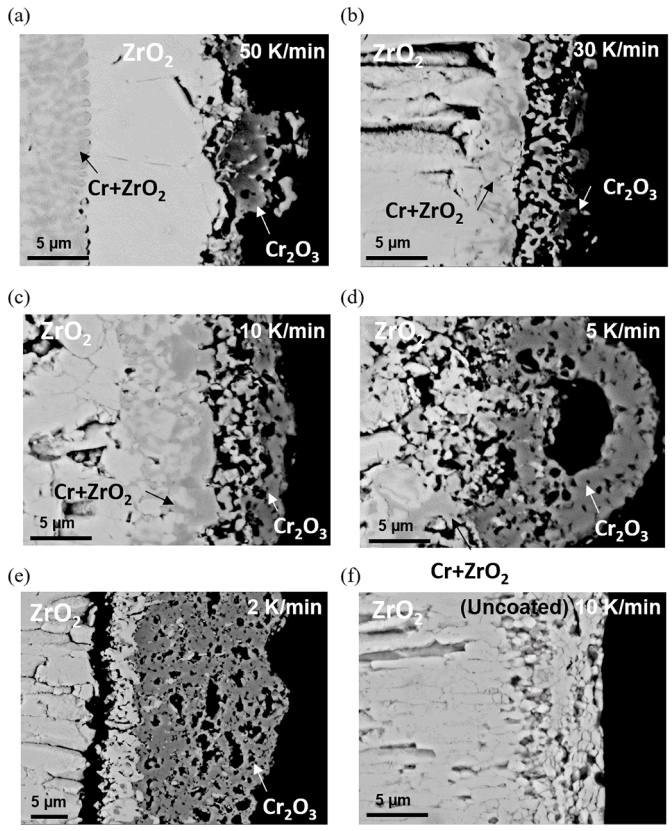

Fig. 9. Cross-sectional SEM-BSE image near the outer coating surface; (a)-(e) Cr-coated Zircaloy-4 specimen. (f) Uncoated Zircaloy-4 specimen.

Fig. 9 shows cross-sectional SEM-BSE images of Cr-coated specimens (2–50 K/min) and one uncoated specimen (10 K/min) magnified to the coating surface. As can be noted, the post-test coating surface of Cr-coated specimens with eutectic reaction (Fig. 9(a)-(d)) can be roughly divided into three types of layers. The EDS quantitative line scan was performed for specimens with a heating rate of 10 K/min to characterize these layers (Fig. 10). The outermost layer was identified as the Cr_2O_3 layer, and the innermost layer was identified as the ZrO_2 layer. A chromium-rich layer with a high concentration of chromium (~90 at%) exists between these two layers, which is a mixture of chromium metal and ZrO_2 phase. The chromium metal should be unreacted coating or reduced metal from the Cr_2O_3 phase by zirconium (Eq. (1)) [17,18], or decomposed from the $ZrCr_2$ intermetallic phase by oxidation (Eq. (2)) [19]. It is worth mentioning that the chromium metal phase was not observed for the specimens with a heating rate of 2 K/min (Fig. 9(e)).

$$2Cr_2O_3 + 3Zr \rightarrow 3ZrO_2 + 4Cr \quad (1)$$

$$ZrCr_2 + 2H_2O \rightarrow ZrO_2 + 2Cr + 2H_2 \quad (2)$$

All Cr_2O_3 layers were porous with many voids in the layer, which is relevant to the failure of coating. The compactness and thickness of the Cr_2O_3 layer depended on the heating rate. Specimens with low heating rate (2–5 K/min) had relatively compact and thick Cr_2O_3 layers compared to specimen with higher heating rate (10–50 K/min), which had relatively thin and non-uniform Cr_2O_3 layers. These results are consistent with the XRD measurements for the surface which showed the existence of various phases (Cr_2O_3, Cr, or ZrO_2) for high heating rates (10–50 K/min) and only a Cr_2O_3 phase for low heating rates (2–5 K/min).

The uncoated specimens (Fig. 9(f)) has a ZrO_2 layer on the surface, which is typical microstructure of oxidized zirconium.

4. Discussion

4.1. Eutectic reaction and heating rate

Chromium can play role in Zr-Cr eutectic reaction when it is in a non-oxidized state and the concentration is larger than the eutectic composition indicated by the phase diagram. Fig. 11 shows the calculated Zr-Cr phase diagram using the ThermoCalc software and TCZR1 database (Zr, Cr, Fe, Nb, Ni, Sn, O, and H). Fig. 11(b) is magnified around the eutectic reaction, and as can be noted, the eutectic melting of zirconium and chromium starts above 1325 °C and the minimum composition of chromium is about 3.7 wt.%. The minimum chromium content decreases for higher temperatures, for instance, it decreases to 3.5 wt.% at 1380 °C, which is the maximum temperature in this study. That is, when the concentration of diffused chromium in the zirconium matrix far from the coating is smaller than 3.5 wt.%, it may not participate in the eutectic reaction. The oxygen content in the metallic layer consists of zirconium and chromium as a result of oxidation and can affect the eutectic composition limit. The calculation of the eutectic composition at 1380 °C was conducted for the Zr-Cr-O system using the ThermoCalc software. The calculated chromium composition limit at 1380 °C tends to decrease for high oxygen concentrations (2.3 wt% for Zr-Cr-1wt%O system and 1.3 wt% for Zr-Cr-2wt%O system).

Therefore, the oxidation of the chromium coating to Cr_2O_3 and the diffusional loss of chromium can reduce the amount of chromium that participates in the eutectic reaction, thereby affecting the extent of the eutectic reaction. In this study, it is observed that the local swelling and area of Zr-$Cr_{prior\ eutectic}$ depend on the heating rate. The extent of local swelling and area of Zr-$Cr_{prior\ eutectic}$ tend to increase with the heating

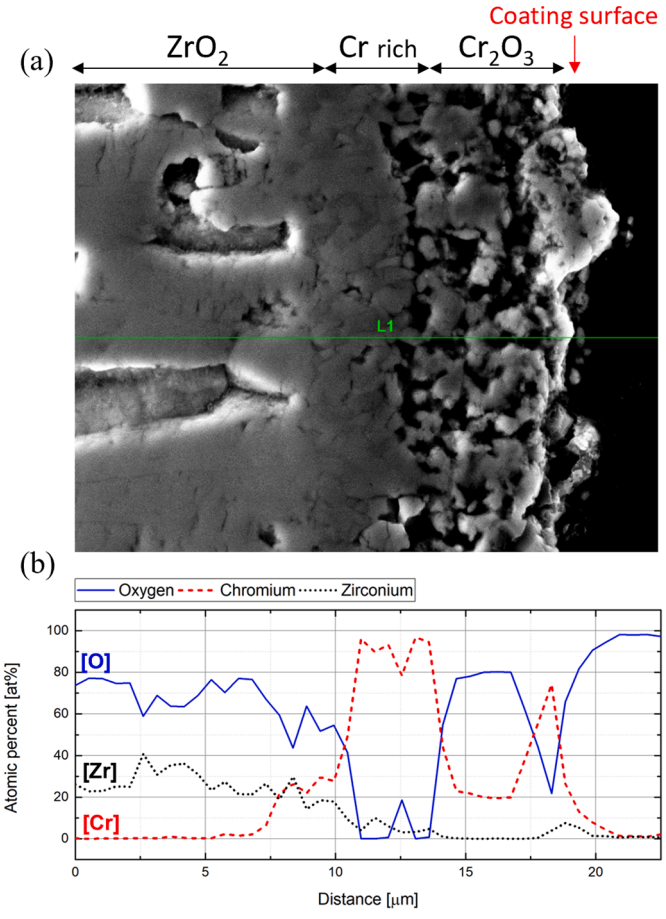

Fig. 10. EDS quantitative line scan at the coating surface of Cr-coated specimens with a heating rate of 10 K/min.

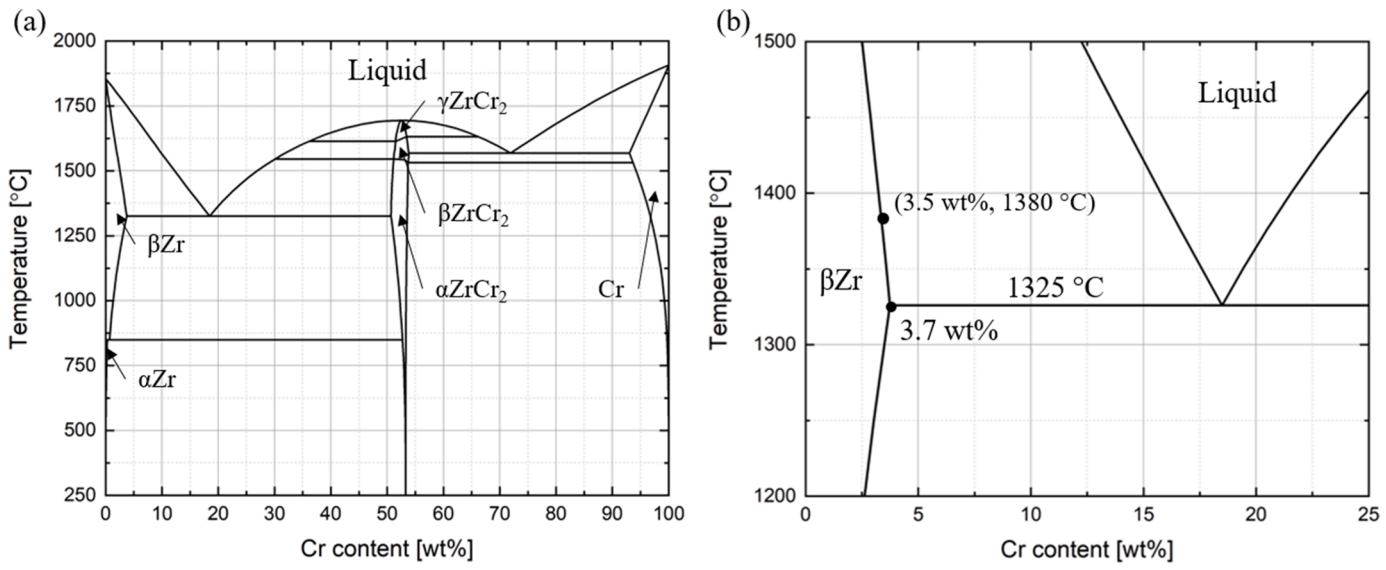

Fig. 11. Calculated Zr-Cr phase diagram using ThermoCalc software and TCZR1 database; (a) Full range. (b) Magnified for eutectic region.

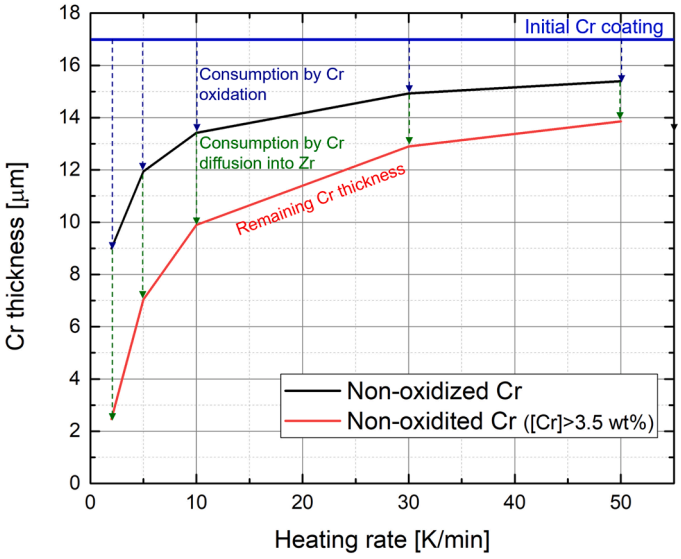

Fig. 12. Estimated remaining metal chromium thickness with original 17 μm thick for different heating rates.

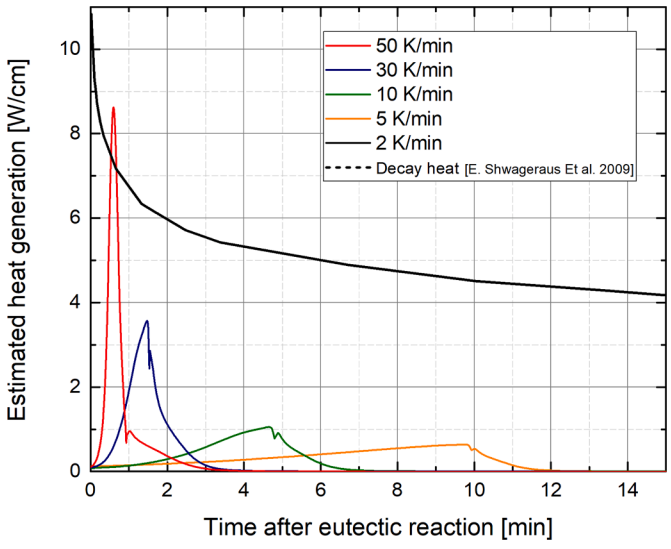

Fig. 13. Estimated equivalent heat generation due to oxidation after eutectic reaction and decay heat after shutdown.

rate and for the lowest heating rate (2 K/min), a post-eutectic microstructure was not observed.

In such a context, the oxidational and diffusional losses of metal chromium under the tested conditions (temperature profile) were calculated for comparison and understanding of the experimental results. The oxidational loss was predicted using the growth kinetic model of Cr_2O_3 layer in a previous study [20]. The diffusional loss was predicted based on the Zr-Cr binary diffusion model developed in another previous study [21]. The Zr-Cr diffusion model calculates the high-temperature diffusion of chromium in zirconium matrix under inert gas conditions and was experimentally validated (1000–1300 °C) in terms of chromium concentration distribution, chromium coating thickness, and $ZrCr_2$ interlayer thickness.

In the case of oxidational loss, the oxidation of chromium under the tested conditions (heating rate) is predicted, and the corresponding consumption of chromium metal is calculated. The growth kinetics of the Cr_2O_3 layer follows a parabolic law as stated in Eqs. (3) and (4). $\delta_{Cr_2O_3}$ is the Cr_2O_3 layer thickness, t is the time, K_0 is the pre-exponential constant, E_A is the activation energy, R is the gas constant (8.314 J/molK), and T is the temperature. The parabolic rate constants given by Steinbrück et al. [20] are as follows: K_0 $2.69 * 10^{-3} m/s^{0.5}$ and E_A $120,000\ J/mol$.

$$\delta_{Cr_2O_3} \quad K_p(T)\cdot\sqrt{t} \tag{3}$$

$$K_p(T) \quad K_0\cdot\exp\left(\frac{E_A}{RT}\right) \tag{4}$$

Using this model, we predicted Cr_2O_3 layer thickness under the experimental conditions (Fig. 2) and estimated the residual non-oxidized chromium metal thickness based on the Cr_2O_3 thickness (Fig. 12). The calculations were conducted at temperatures up to 1325 °C, just before the eutectic onset temperature, and the residual metal thickness was estimated considering the Pilling-Bedworth ratio of Cr_2O_3 (2.03) [22]. The results in Fig. 12 indicate that the estimated non-oxidized chromium thickness decreases with a lower heating rate, which is attributed to a longer oxidation time.

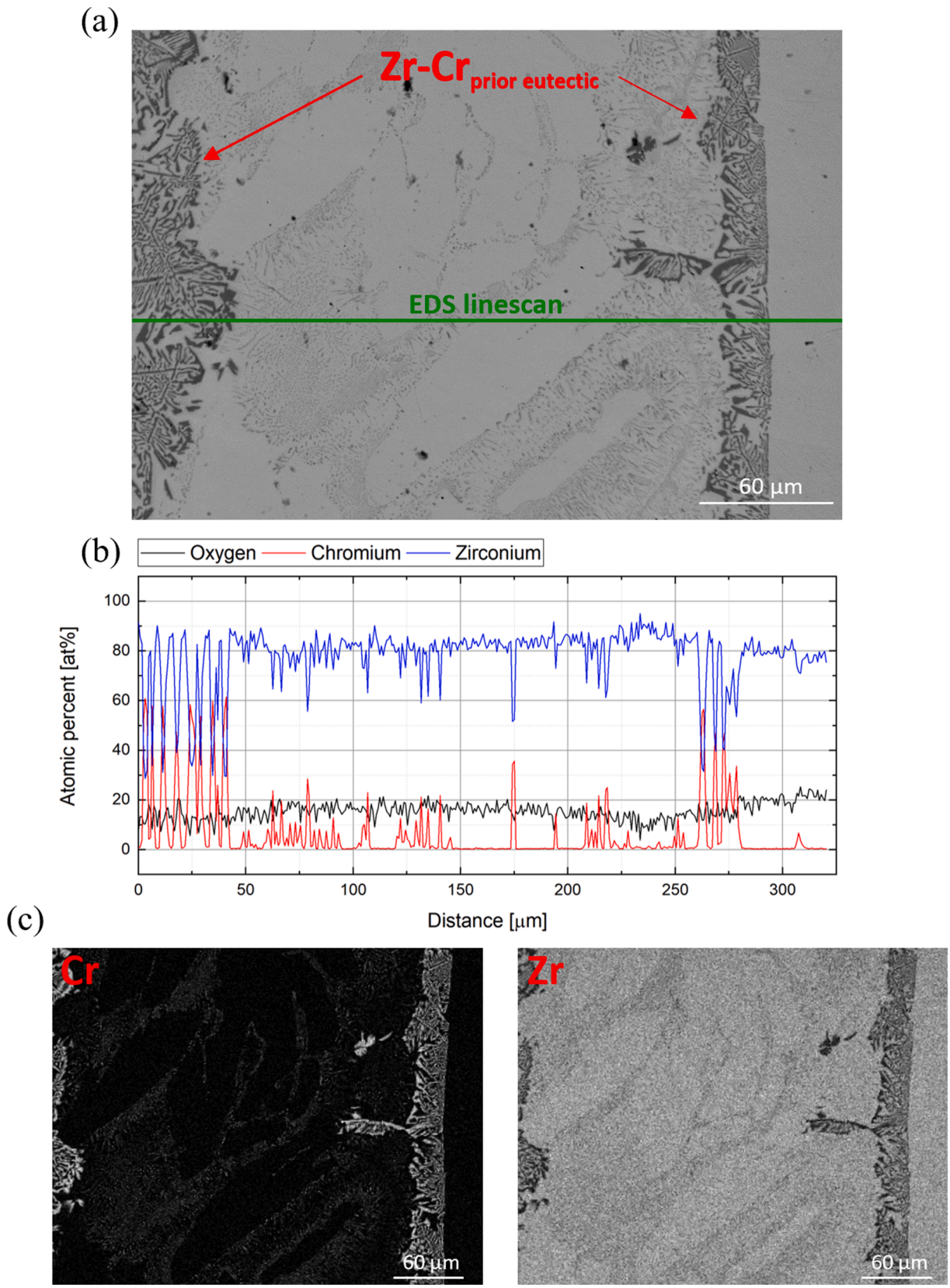

Fig. A1. Microstructure of the chromium-rich region in specimen with heating rate of 10 K/min; (a) SEM-BSE image. (b) EDS line scan result. (c) EDS mapping result.

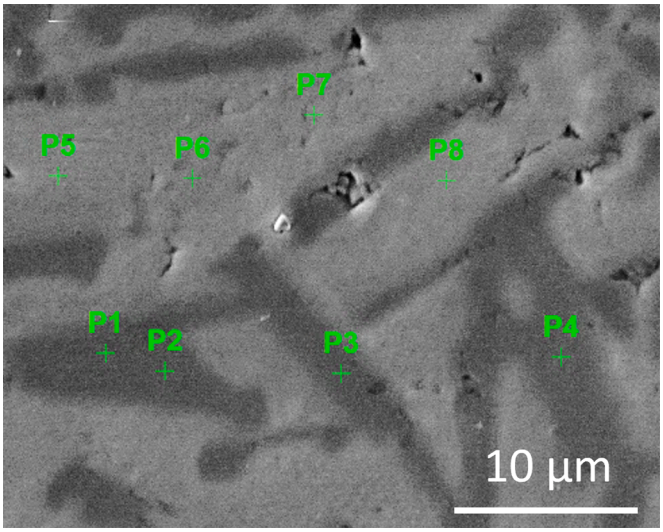

Fig. A2. EDS measurement (Table 1) positions of Cr-coated specimens with heating rate of 10 K/min.

Table. A1
EDS measurement results.

Point No.	Oxygen [at%]	Chromium [at%]	Zirconium [at%]
1	10.75	58.93	30.00
2	10.37	56.36	33.05
3	12.40	57.76	29.63
4	11.96	56.56	31.19
5	17.10	0.75	80.26
6	17.19	2.21	79.15
7	15.86	0.45	82.20
8	18.57	0.86	78.81

In the case of diffusional loss, the chromium concentration profile under the tested conditions (heating rate) was predicted and the amount of diffused chromium that does not exceed the eutectic composition limit (3.5 wt% chromium) was calculated. It was assumed that the diffusional kinetics of chromium in inert gas (diffusion model) and oxygen (used in this study) are comparable. The calculation was performed at up to 1325 °C, just before the eutectic onset temperature, and the calculated amount of diffused chromium was converted into effective diffusional loss in coating thickness. The composition limit was set to 3.5 wt% but it could be changed according to the oxygen content, as mentioned above. Therefore, the practical diffusional loss is expected to be smaller than the presented results because of the oxygen content in specimen due to oxidation after coating failure.

The chromium thickness that is non-oxidized and above the eutectic composition limit was calculated and is depicted in Fig. 12 (non-oxidized ([C*r*]>3.5 wt%)). As can be noted, it decreases for a lower heating rate because of longer exposure to oxidation and diffusion. These results are in line with the observation that the impacts of eutectic reaction, such as weight gain escalation, surface morphology, and local swelling, were more significant at higher heating rates. In the case of the 50 K/min specimen, which is the fastest heating rate, most of the coating (>80%) remains in a non-oxidized state and above the composition limit while about 40% of the coating remains for specimen with a 5 K/min heating rate. In the case of the slowest heating rate (2 K/min) specimen, a relatively low portion (~15%) of the coating is expected to remain in a non-oxidized state and above the composition limit. This prediction is not completely consistent with the experimental results that showed no weight gain rate escalation or Zr-$Cr_{prior\ eutectic}$ microstructure due to eutectic reaction. This is thought to be because coating lost its protectiveness at around 1280 °C (Fig. 4(b)) and leads to a transition in oxidation kinetics from the existing parabolic growth behavior (Eq. (3)), resulting in a higher portion of chromium oxidized than stated in the predicted results.

4.2. Heat generation after eutectic reaction

The high weight gain rate observed after eutectic reaction corresponds to the high oxidation rate of the metal (i.e., zirconium or chromium). The oxidation of zirconium and chromium is an exothermic reaction, hence, a large amount of oxidation heat could be generated due to accelerated oxidation. When the oxidation heat exceeds the capacity of the cooling system, the temperature of the cladding rises, thereby resulting in runaway oxidation and meltdown of the core. The runaway oxidation and melting of cladding due to the temperature escalation of cladding caused by rapid oxidation was described in previous studies [23,24]. It is therefore important to quantitatively study the magnitude of oxidation heat corresponding to the observed high weight gain rate after eutectic reaction. Hence, in this section, heat generation according to the weight gain rate is estimated and compared with the decay heat of the reactor core after shutdown. It was assumed that the oxidation kinetics in steam (a more prototypical atmosphere) and oxygen (used in this study) are comparable. The analysis was performed based on the geometry of typical nuclear fuel cladding, and it was assumed that the reaction rate per unit area was the same as that of the plate-shaped specimens used in the experiment.

The heat generation due to the weight gain rate can be calculated by multiplying it by the oxidation heat ($\frac{dQ}{dm}$) of the metal (Eq. (5)). The oxidation heat of zirconium with steam is 6.4 $J/mgZr$ at 1200 °C based on the HSC chemistry [25] and using that, the unit weight gain rate of 1 mg/min can be converted into a heat generation of 0.107 W.

$$\dot{Q} \quad \frac{dm}{dt} * \frac{dQ}{dm} \quad 1\ \mathrm{mg/min} * 6.4\ \mathrm{J/mg} \quad 0.107\ \mathrm{W} \tag{5}$$

The heat flux can be obtained by dividing the calculated heat generation by the surface area of the specimen (Eq. (6)). Considering that the area of each side of the specimen is 1.5 cm^2 and the specimen was double-sided oxidized, and it has edge area about 0.325 cm^2, the heat flux of 0.0322 W/cm^2 corresponding to 1 mg/cm^2 is obtained.

$$Q'' \quad \dot{Q}/A \quad \dot{Q}/(2 * 1.5 + 0.325\ \mathrm{cm}^2) \quad 0.0322\ \mathrm{W/cm}^2 \tag{6}$$

The linear heat generation rate of the fuel rod in tube shape with a diameter of 0.95 cm was calculated by multiplying heat flux by the circumference length (Eq. (7)). Consequently, the unit weight gain rate of 1 mg/min due to oxidation of zirconium corresponds to the linear heat generation of 0.096 W/cm of a fuel rod.

$$Q' \quad Q'' * 2\pi r \quad Q'' * \pi * 0.95\ \mathrm{cm} \quad 0.096\ \mathrm{W/cm} \tag{7}$$

In the case of weight gain due to oxidation of chromium, the linear heat generation of 0.054 W/cm can be obtained by repeating Eqs. (5)-(7) considering that the oxidation heat of chromium with steam is 3.6 $J/mgCr$ at 1200 °C based on the HSC chemistry [25].

The linear heat generation corresponding to the measured weight gain rate after the eutectic reaction of each specimen in Fig. 5 was calculated and compared with decay heat after the shutdown (Fig. 13). The oxidation could take place in both zirconium and chromium, but zirconium is preferentially oxidized in the presence of both metals [18] and its oxidation rate is about 100 times faster than that of chromium [20]. Hence, all measured weight gain was assumed to be due to the oxidation of zirconium in the calculation. In addition to that, nuclear fuel has an axial/radial temperature gradient, so the temperature of some part may not exceed the eutectic temperature, but for the simplicity, we assumed that the eutectic reaction and oxidation was take place in whole surface. The decay heat is about 6% of the normal power right after the shutdown and decreases over time. The calculated fraction of decay heat compared to the normal power over time by

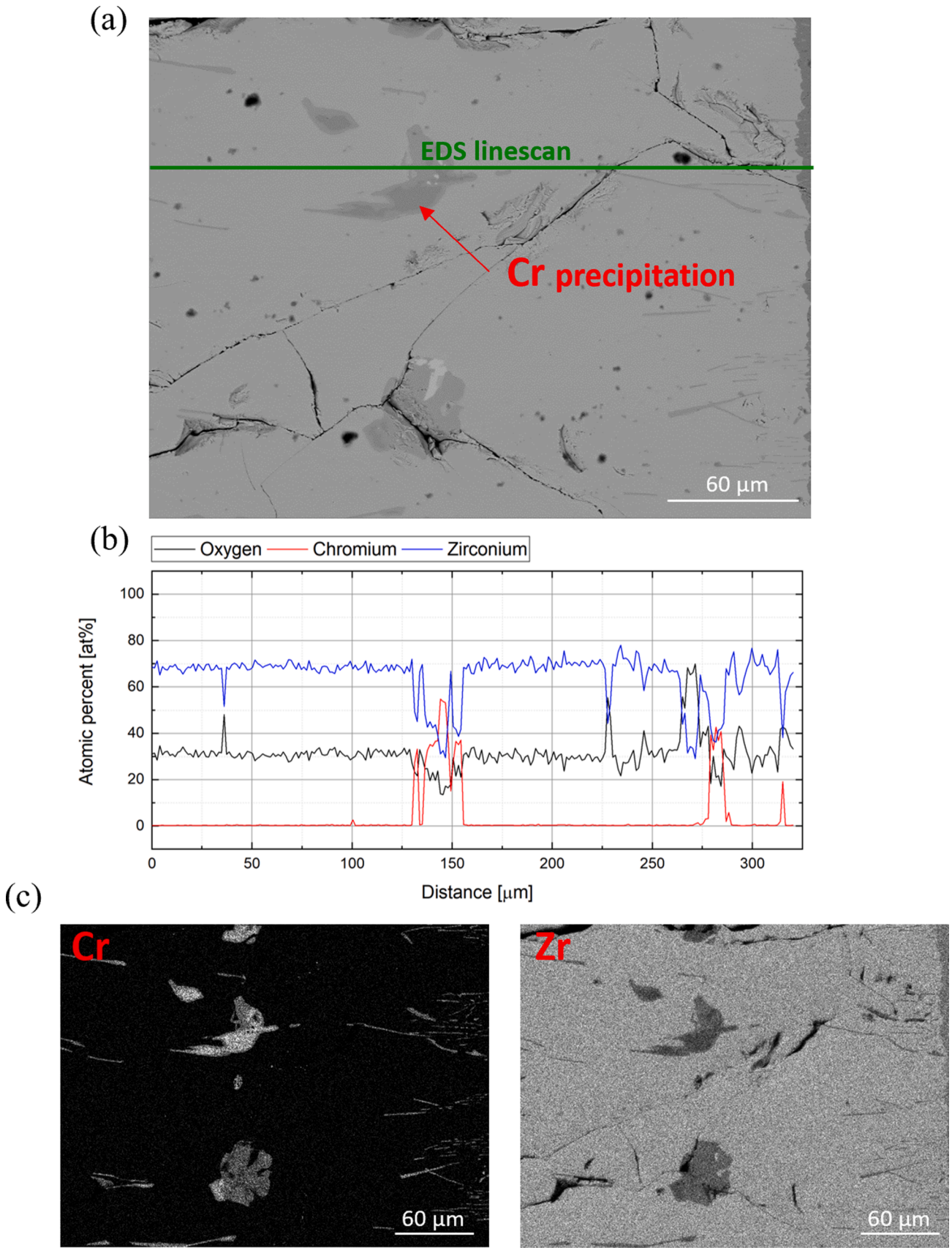

Fig. A3. Microstructure of the chromium-rich region in specimen with a heating rate of 2 K/min; (a) SEM-BSE image. (b) EDS line scan result. (c) EDS mapping result.

Shwageraus et al. [26] was extracted and used for the comparison. The normal power was set to 20 kW/m.

As can be noted in Fig. 13, the peak heat generation rate due to oxidation increases with the heating rate, and in the case of 50 K/min, which is the highest heating rate, even exceeds the decay heat after shutdown. These results imply that the accelerated heat generation due to failure of coating above the eutectic temperature could play an important role for the coolability of the core. The exact temperature rise could be calculated using nuclear fuel computational simulation codes (e.g., FRAPTRAN) in a further study. It is worth mentioning that the maximum heating rate of this study (50 K/min) is relatively low compared to that of design-based accidents (DBAs) or beyond DBAs (about 200–300 K/min). Since the weight gain rate and corresponding heat generation after eutectic increase as the heating rate increases, the heat generation under prototypical heating rate would be more noticeable than in this study.

5. Conclusion

In this study, Cr-coated Zircaloy-4 cladding specimens were subjected to transient oxidation experiments at temperatures up to 1380 °C under five different heating rates (2–50 K/min) in an oxygen environment. TGA was used to in-situ measure the mass change of the specimens, and SEM, XRD, and EDS were used for post-test analysis. The thickness of the remaining chromium metal was calculated using a combination of the parabolic oxidation correlation and the Zr-Cr binary diffusion model, and it was compared with the experimental results. Furthermore, this study estimated the amount of heat generated due to oxidation, which corresponds to the measured weight gain rate after the eutectic reaction and compared it with the amount of decay heat after shutdown.

CRediT authorship contribution statement

Dongju Kim: Methodology, Software, Validation, Formal analysis, Investigation, Resources, Writing – original draft, Writing – review & editing. **Martin Steinbrück:** Conceptualization, Methodology, Investigation, Resources, Writing – review & editing, Supervision, Project administration, Funding acquisition. **Mirco Grosse:** Conceptualization, Methodology, Investigation, Resources, Writing – review & editing, Supervision, Project administration, Funding acquisition. **Chongchong Tang:** Data curation, Resources, Writing – review & editing. **Youho Lee:** Methodology, Resources, Writing – review & editing.

Declaration of Competing Interest

The authors declare that they have no known competing financial interests or personal relationships that could have appeared to influence the work reported in this paper.

Data availability

Data will be made available on request.

Acknowledgement

This study was supported by the HGF German nuclear safety program NUSAFE at KIT and the Nuclear Global Internship Program through the Korea Nuclear International Cooperation Foundation (KONICOF) funded by the Ministry of Science and ICT (NRF-2022M2C7A1A03062813). We thank U. Stegmaier for her technical support during experiments.

Appendix A: Analysis of Chromium-rich Regions of Specimens

Specimens with weight gain rate escalation near the Zr-Cr eutectic temperature (heating rate$\geq$ 5 K/min) (Fig. 8(b2)-(e2)) have similar microstructures of the chromium-rich regions. The SEM-BSE image, EDS line scan, and EDS mapping results for the chromium-rich regions in specimen with a heating rate of 10 K/min are presented in Fig. A1. As can be noted, a relatively large and prominent chromium precipitation exists on both sides, and there is fine chromium precipitation at the center between them. Additional EDS quantitative analysis was conducted (Fig. A2 and Table. A1) for the large chromium precipitation and it demonstrates that the observed chromium-rich region is $ZrCr_2$ precipitation distributed in the zirconium matrix. Such microstructure was formed by the decomposition of the Zr-Cr liquid into $ZrCr_2$ intermetallic and zirconium phases during cooling, and it can also be found in past studies (Zr-$Cr_{\text{prior eutectic}}$) [13].

Although the fine precipitation was difficult to quantitatively analyze due to its small size, it is thought to exist in the form of $ZrCr_2$, a stable intermetallic phase between zirconium and chromium (Fig. 11 (a)). The average chromium concentration in the fine precipitation region was about 2.1 wt%, which is lower than the eutectic composition limit (~3.5 wt%). Therefore, it seems that some portion of diffused chromium that existed as a solid solution in zirconium did not participate in the eutectic reaction due to its low concentration and precipitated during cooling.

The SEM-BSE image, EDS line scan, and EDS mapping results for the chromium-rich regions in specimens with a heating rate of 2 K/min are presented in Fig. A3. As can be noted, Zr-$Cr_{\text{prior eutectic}}$ structure ($ZrCr_2$ precipitation phase heterogeneously exists in the zirconium matrix) was not observed. Instead, a few relatively big $ZrCr_2$ precipitations can be found near the center. The average chromium concentration in the overall unoxidized zirconium matrix region was about 1.7 wt%, which was lower than the eutectic composition limit (~3.5 wt%). Therefore, it seems that because of the low chromium concentration in the unoxidized zirconium matrix, the diffused chromium did not participate in the eutectic reaction and precipitated during cooling.

References

[1] R.V. Umretiya, B. Elward, D. Lee, M. Anderson, R.B. Rebak, J.V. Rojas, Mechanical and chemical properties of PVD and cold spray Cr-coatings on Zircaloy-4, J. Nucl. Mater. 541 (2020), 152420.
[2] F. Fejt, M. Sevecek, J. Frýbort, O. Novak, Study on neutronics of VVER-1200 with accident tolerant fuel cladding, Ann. Nucl. Energy 124 (2019) 579–591.
[3] H. Yook, K. Shirvan, B. Phillips, Y. Lee, Post-LOCA ductility of Cr-coated cladding and its embrittlement limit, J. Nucl. Mater. 558 (2022), 153354.
[4] J. Yang, M. Steinbrück, C. Tang, M. Große, J. Liu, J. Zhang, D. Yun, S. Wang, Review on chromium coated zirconium alloy accident tolerant fuel cladding, J. Alloys Compd. 895 (2022), 162450.
[5] G. Bourdon, M. Ševecek, J. Krejčí, L. Cvrček, High-temperature steam and air oxidation of chromium-coated optimized Zirlo™, Acta Polytechnica CTU Proc. 24 (2019) 1–8.
[6] J. Liu, Z. Cui, Z. Hao, D. Ma, J. Lu, Y. Cui, C. Li, W. Liu, S. Xie, P. Hu, P. Huang, G. Bai, D. Yun, Steam oxidation of Cr-coated Sn-containing Zircaloy solid rod at 1000 °C, Corros. Sci. 190 (2021), 109682.
[7] H. Yeom, B. Maier, G. Johnson, T. Dabney, M. Lenling, K. Sridharan, High temperature oxidation and microstructural evolution of cold spray chromium coatings on Zircaloy-4 in steam environments, J. Nucl. Mater. 526 (2019), 151737.
[8] J. Liu, C. Tang, M. Steinbrück, J. Yang, U. Stegmaier, M. Große, D. Yun, H.J. Seifert, Transient experiments on oxidation and degradation of Cr-coated Zircaloy in steam up to 1600 °C, Corros. Sci. 192 (2021), 109805.
[9] J.-S. Jiang, D.-Q. Wang, M.-Y. Du, X.-F. Ma, C.-X. Wang, X.-J. He, Interdiffusion behavior between Cr and Zr and its effect on the microcracking behavior in the Cr-coated Zr-4 alloy, Nucl. Sci. Tech. 32 (12) (2021) 134.
[10] H.-J. Lu, W.-B. Wang, N. Zou, J.-Y. Shen, X.-G. Lu, Y.-L. He, Thermodynamic modeling of Cr–Nb and Zr–Cr with extension to the ternary Zr–Nb–Cr system, Calphad 50 (2015) 134–143.
[11] N. Chaari, J. Bischoff, K. Buchanan, C. Delafoy, P. Barberis, J. Augereau, K. Nimishakavi, The behavior of Cr-coated zirconium alloy cladding tubes at high temperatures, in: A.T. Motta, S.K. Yagnik (Eds.), Zirconium in the Nuclear Industry:

19th International Symposium, ASTM International, West Conshohocken, PA, 2021, pp. 189–210.
[12] M. Steinbrück, U. Stegmaier, M. Große, L. Czerniak, E. Lahoda, R. Daum, K. Yueh, High-temperature oxidation and quenching of chromium-coated zirconium alloy ATF cladding tubes with and w/o pre-damage, J. Nucl. Mater. 559 (2022), 153470.
[13] J.-.C. Brachet, T. Guilbert, M.Le Saux, J. Rousselot, G. Nony, C. Toffolon-Masclet, A. Michau, F. Schuster, H. Palancher, J. Bischoff, J. Augereau, E. Pouillier, Behavior Of Cr-Coated M5 claddings during and after high temperature steam oxidation from 800°C Up To 1500°C (Loss-Of-Coolant Accident & Design Extension Conditions), 2018.
[14] D. Kim, M. Steinbrück, M. Grosse, C. Tang, Effect of heating rates on the eutectic reaction and oxidation behavior of Cr-coated zircaloy-4 accident tolerant fuel cladding, in: ICAPP 2023 /38th KAP Conference, 2023. Gyeongju, Korea.
[15] J. Liu, M. Steinbrück, M. Große, U. Stegmaier, C. Tang, D. Yun, J. Yang, Y. Cui, H. J. Seifert, Systematic investigations on the coating degradation mechanism during the steam oxidation of Cr-coated Zry-4 at 1200°C, Corros. Sci. 202 (2022), 110310.
[16] M. Steinbrück, M. Große, C. Tang, J. Stuckert, Limiting degradation mechanisms for high-temperature oxidation resistance of promising ATF cladding solutions, TopFuel 2022, Raleigh, NC, 2022.
[17] H.-.B. Ma, J. Yan, Y.-.H. Zhao, T. Liu, Q.-.S. Ren, Y.-.H. Liao, J.-.D. Zuo, G. Liu, M.-.Y. Yao, Oxidation behavior of Cr-coated zirconium alloy cladding in high-temperature steam above 1200°C, npj Mater. Degradat. 5 (1) (2021) 7.
[18] X. Han, C. Chen, Y. Tan, W. Feng, S. Peng, H. Zhang, A systematic study of the oxidation behavior of Cr coatings on Zry4 substrates in high temperature steam environment, Corros. Sci. 174 (2020), 108826.
[19] J.-.C. Brachet, E. Rouesne, J. Ribis, T. Guilbert, S. Urvoy, G. Nony, C. Toffolon-Masclet, M.Le Saux, N. Chaabane, H. Palancher, A. David, J. Bischoff, J. Augereau, E. Pouillier, High temperature steam oxidation of chromium-coated zirconium-based alloys: kinetics and process, Corros. Sci. 167 (2020), 108537.
[20] M. Steinbrück, M. Große, C. Tang, J. Stuckert, Limiting degradation mechanisms for high-temperature oxidation resistance of promising ATF cladding solutions, Proceedings | TopFuel 2022 Light Water Reactor Fuel Performance Conference | Raleigh, NC, October 9-13, 2022, American Nuclear Society (ANS), Raleigh, NC, USA, 2022, pp. 251–260.
[21] D. Kim, Y. Lee, Development and validation of Cr diffusion model for coated zircaloy accident tolerant fuel cladding, Transactions of the Korean Nuclear Society Spring Meeting, Jeju, Korea, 2022.
[22] S. Sun, Z. Zhou, L. Zhang, R. Tang, Oxidation behavior and stress corrosion cracking susceptibility of Fe27Ni16Cr3.5Al based AFA Alloy in supercritical water, Mater. Res. Express 5 (2018).
[23] J. Stuckert, M. Steinbrueck, J. Kalilainen, T. Lind, J. Birchley, Experimental and modelling results of the QUENCH-18 bundle experiment on air ingress, cladding melting and aerosol release, Nucl. Eng. Des. 379 (2021). Art.-Nr.
[24] M. Steinbrück, M. Große, L. Sepold, J. Stuckert, Synopsis and outcome of the QUENCH experimental program, Nucl. Eng. Des. 240 (7) (2010) 1714–1727.
[25] HSC Chemistry® 10, Metso Outotec, Finland, 1974–2023.
[26] E. Shwageraus, P. Hejzlar, Decay heat in fast reactors with transuranic fuels, Nucl. Eng. Des. 239 (12) (2009) 2646–2653.